Exploring partial μ-τ reflection symmetry at DUNE and Hyper-Kamiokande

Kaustav Chakraborty,[1,2,*] K. N. Deepthi,[1,†] Srubabati Goswami,[1,‡] Anjan S. Joshipura,[1,§] and Newton Nath[3,4,¶]

[1]*Theoretical Physics Division, Physical Research Laboratory, Ahmedabad 380009, India*

[2]*Discipline of Physics, Indian Institute of Technology, Gandhinagar 382355, India*

[3]*Institute of High Energy Physics, Chinese Academy of Sciences, Beijing 100049, China*

[4]*School of Physical Sciences, University of Chinese Academy of Sciences, Beijing 100049, China*

(Received 12 April 2018; revised manuscript received 11 October 2018; published 31 October 2018)

We study the origin, consequences, and testability of a hypothesis of "partial μ-τ" reflection symmetry. This symmetry predicts $|U_{\mu i}| = |U_{\tau i}| (i = 1, 2, 3)$ for a single column of the leptonic mixing matrix U. Depending on whether this symmetry holds for the first or second column of U, different correlations between θ_{23} and δ_{CP} can be obtained. This symmetry can be obtained using discrete flavor symmetries. In particular, all of the subgroups of SU(3) with three-dimensional irreducible representation, which are classified as class C or D, can lead to partial μ-τ reflection symmetry. We show how the predictions of this symmetry compares with the allowed area in the $\sin^2\theta_{23}$-δ_{CP} plane as obtained from the global analysis of neutrino oscillation data. Furthermore, we study the possibility of testing these symmetries at the proposed DUNE and Hyper-Kamiokande (HK) experiments (T2HK, T2HKK), by incorporating the correlations between θ_{23} and δ_{CP} that are predicted by the symmetries. We find that when the simulated data of DUNE and HK are fitted with the symmetry predictions, the $\theta_{23} - \delta_{CP}$ parameter space gets largely restricted near the charge parity conserving values of δ_{CP}. Finally, we illustrate the capability of these experiments to distinguish between the two cases leading to partial μ-τ symmetry, namely $|U_{\mu 1}| = |U_{\tau 1}|$ and $|U_{\mu 2}| = |U_{\tau 2}|$.

DOI: 10.1103/PhysRevD.98.075031

I. INTRODUCTION

Considerable theoretical and experimental efforts are being devoted towards predicting and determining the unknowns of the leptonic sectors, namely the charge parity (CP) violating phase, octant of the atmospheric mixing angle θ_{23} [i.e., $\theta_{23} < 45°$, named as lower octant (LO) or $\theta_{23} > 45°$ named as upper octant (HO)], and the neutrino mass hierarchy [i.e., the sign of Δm^2_{31}, $\Delta m^2_{31} > 0$ known as normal hierarchy (NH) and $\Delta m^2_{31} < 0$ known as inverted hierarchy (IH)]. Symmetry based approaches have been quite successful in predicting the interrelations among these quantities and the structure of the leptonic mixing matrix as discussed in Refs. [1–5] and the references therein. General approaches along this line assume some individual residual symmetries of the leptonic mass matrices that could arise from the breaking of some of the bigger symmetry of the leptonic interactions. One such symmetry, called μ-τ reflection symmetry, originally discussed by Harrison and Scott in Ref. [6], leads to very successful predictions of mixing angles that are close to the present experimental knowledge. This symmetry may be stated as an equality of moduli of the leptonic mixing matrix U:

$$|U_{\mu i}| = |U_{\tau i}|, \tag{1}$$

for all of the columns $i = 1, 2, 3$. Both the origin and consequences of this relation have been discussed in [7–22].

Using the standard Particle Data Group (PDG) [23] parametrization of the matrix U

*kaustav@prl.res.in
†deepthi@prl.res.in
‡sruba@prl.res.in
§anjan@prl.res.in
¶newton@ihep.ac.cn

$$U = U(\theta_{23})U(\theta_{13},\delta_{CP})U(\theta_{12}) = \begin{bmatrix} c_{12}c_{13} & s_{12}c_{13} & s_{13}e^{-i\delta_{CP}} \\ -s_{12}c_{23} - c_{12}s_{23}s_{13}e^{i\delta_{CP}} & c_{12}c_{23} - s_{12}s_{23}s_{13}e^{i\delta_{CP}} & s_{23}c_{13} \\ s_{12}s_{23} - c_{12}c_{23}s_{13}e^{i\delta_{CP}} & -c_{12}s_{23} - s_{12}c_{23}s_{13}e^{i\delta_{CP}} & c_{23}c_{13} \end{bmatrix}, \tag{2}$$

one finds two well-known predictions

$$\theta_{23} = \frac{\pi}{4}, \qquad s_{13}\cos\delta_{CP} = 0. \tag{3}$$

Equation (3) suggests a maximal θ_{23}, which is allowed within 1σ by the global fits to neutrino observables [24–26]. Additionally, it allows a nonzero θ_{13}, unlike the simple μ-τ symmetry that predicts vanishing θ_{13} [27–32], see recent review [33] and references therein. Here, for $\theta_{13} \neq 0$, one gets $\delta_{CP} = \pm\frac{\pi}{2}$ using Eq. (3). Both of these predictions are in accord with the global fit of all neutrino data. However, a sizeable range is still allowed at 3σ. Note that, the best fit value of θ_{23} in the global fit deviates from the maximal value for either mass hierarchy. Such deviations can be regarded as a signal for the departure from the μ-τ reflection symmetry. A theoretically well-motivated possibility is to assume a "partial μ-τ" reflection symmetry [34] and assume that Eq. (1) holds only for a single column[1] of U. Assuming that it holds for the third column, one gets the maximal θ_{23} and δ_{CP} remains unrestricted. These correlations are found from Eq. (2) in respective cases $i = 1$ and $i = 2$ to be

$$\cos\delta_{CP} = \frac{(c_{23}^2 - s_{23}^2)(c_{12}^2 s_{13}^2 - s_{12}^2)}{4c_{12}s_{12}c_{23}s_{23}s_{13}}, \qquad (|U_{\mu 1}| = |U_{\tau 1}|), \qquad C_1, \tag{4}$$

$$\cos\delta_{CP} = \frac{(c_{23}^2 - s_{23}^2)(c_{12}^2 - s_{12}^2 s_{13}^2)}{4c_{12}s_{12}c_{23}s_{23}s_{13}}, \qquad (|U_{\mu 2}| = |U_{\tau 2}|), \qquad C_2. \tag{5}$$

These equations correlate the sign of $\cos\delta_{CP}$ to the octant of θ_{23}. θ_{23} in the first (second) octant leads to a negative (positive) value of $\cos\delta_{CP}$ in the case of Eq. (4). It exactly predicts the opposite behavior for Eq. (5). The exact quadrant of δ is still not fixed by these equations, but it can also be determined from symmetry considerations [20]. These correlations were also obtained in [35,36] in the context of Z_2 and $\overline{Z_2}$ symmetries.[2] Henceforth, we refer to these correlations as C_1 and C_2, respectively. The above equations also indirectly lead to information on the neutrino mass hierarchy since the best fit values of θ_{23} lie in the first (second) octant in the case of the normal (inverted) hierarchy, according to the latest global fits reported in [24–26]. Thus, precise verification of the above equations is of considerable importance, and the long baseline experiments can provide a way for such study. A similar study has been performed in the context of the NOνA and T2K experiments in [38–40].

In this paper, we consider the testability of these relations at the forthcoming long baseline experiments of the Deep Under-ground Neutrino Experiment (DUNE) and Hyper-Kamiokande (HK). These potential high-statistics experiments will overcome the parameter degeneracies faced by the current experiments and lead us in to an era of precision measurements of the oscillation parameters [41–50]. Because of this, these experiments are ideal to test the parameter correlations like the ones given in the Eqs. (4), (5). In the following, we obtain the allowed parameter range in the δ_{CP}-$\sin^2\theta_{23}$ plane by fitting the symmetry relations embodied in Eqs. (4), (5) to the simulated DUNE and HK data. We also discuss whether the correlations C_1 [Eq. (4)] and C_2 [Eq. (5)] can be distinguished at DUNE and HK. Recent studies on testing various models from future experiments can be found, for instance, in [51–59].

We begin by first discussing the origin of partial μ-τ reflection symmetry. After which, in Sec. II, we elaborate on the robustness of the resulting predictions in a large class of models based on flavor symmetry. We give a brief overview of the experiments and simulation details in Sec. III. In Sec. IV, we perform a phenomenological analysis of the testability of the above symmetries in the DUNE and HK data. We use the extra correlations predicted by the symmetry in fitting the simulated data of these experiments, and we obtain the allowed areas in the δ_{CP}-$\sin^2\theta_{23}$ plane. In subsection IV B, we discuss the possibility of differentiating between the two symmetries—C_1 and C_2. We draw our conclusions in Sec. V.

II. PARTIAL μ-τ REFLECTION SYMMETRY AND DISCRETE FLAVOR SYMMETRIES

Here, we briefly review the general approach based on flavor symmetry to emphasize that partial μ-τ reflection symmetry is a generic prediction of almost all such schemes, barring a few exceptions. Basic approaches assume groups G_ν and G_l as the residual symmetries of the neutrino mass matrix M_ν and the charged lepton mass matrix $M_l M_l^\dagger$, respectively. Both of these groups are assumed to arise from the breaking of some unitary discrete group G_f. The $U_{\rm PMNS}$ matrix U gets fixed up to the neutrino Majorana phases if

[1] If it holds for any two columns, then by unitarity, it holds for the third as well.

[2] See the review article [37] for references on other similar sum rules and their testability.

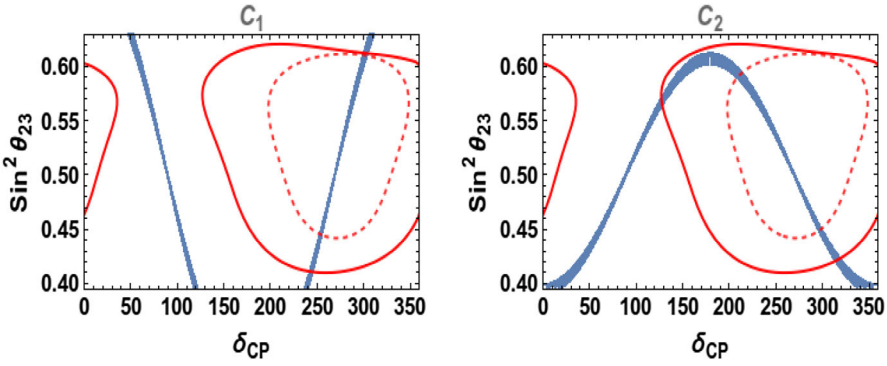

FIG. 1. The thick blue lines show the correlation plots in the $\sin^2\theta_{23}$-δ_{CP} plane as predicted by the symmetry relations. The left (right) panel correspond to Eq. (4) [Eq. (5)]. The solid(dashed) red curves represent the 3σ allowed parameter space as obtained by the global analysis of data by the Nu-fit Collaboration [26,63] considering the hierarchy to be NH(IH), respectively.

it is further assumed that $G_\nu = Z_2 \times Z_2$ and $G_l = Z_n, n \geq 3$. In addition, if we demand that all of the predicted mixing angles are nonzero, then the following unique form is predicted for almost all the discrete groups G_f [60,61],

$$U \equiv U_{\rm gen}(\theta_n) = \frac{1}{\sqrt{3}} \begin{pmatrix} \sqrt{2}\cos\theta_n & 1 & \sqrt{2}\sin\theta_n \\ \sqrt{2}\cos\left(\theta_n - \frac{2\pi}{3}\right) & 1 & \sqrt{2}\sin\left(\theta_n - \frac{2\pi}{3}\right) \\ \cos\left(\theta_n - \frac{4\pi}{3}\right) & 1 & \sqrt{2}\sin\left(\theta_n - \frac{4\pi}{3}\right) \end{pmatrix}, \tag{6}$$

where $\theta_n \equiv \frac{\pi a}{n}$ is a discrete angle with $a = 0, 1, 2 \ldots \frac{n}{2}$. Here, we have not shown the unphysical phases that can be absorbed in defining charged lepton fields and unpredicted Majorana phases. All of the discrete subgroups of SU(3) with three dimensional irreducible representation are classified as class C or D and five exceptional groups [62]. Equation (6) follows in all of the type D groups taken as G_f. Type C groups lead instead to democratic mixing, which shows full μ-τ reflection symmetry but predicts a large reactor angle. Equation (6) arises even if G_f is chosen as a discrete subgroup of $U(3)$, having the same textures as class D groups [61].

Equation (6) displays partial μ-τ reflection symmetry for the second column for all the values of $\theta_n \neq 0, \frac{\pi}{2}$. In the latter case, one gets total μ-τ reflection symmetry, but at the same time, one of the mixing angles is predicted to be zero and one would need to break the assumed residual symmetries to get the correct mixing angles. More importantly, Eq. (6) essentially being a real matrix also predicts a trivial Dirac CP phase $\delta_{CP} = 0$ or π. Equation (5) in this case implies a correlation among angles. A nonzero CP phase and partial μ-τ symmetry in other columns can arise in an alternative but less predictive approach, in which the residual symmetry of the neutrino mass matrix is taken as Z_2 instead of $Z_2 \times Z_2$. In this case, one can obtain the following mixing matrix U with a proper choice of residual symmetries

$$U = U_{\rm gen}(0) U_{ij}, \tag{7}$$

where U_{ij} denotes a unitary rotation either in the ijth plane corresponding to partial symmetry in the kth $(i \neq j \neq k)$ column. Examples of the required residual symmetries are discussed in [1–5], and a minimal example of this occurs with $G_f = S_4$.

The partial μ-τ symmetries obtained this way also lead to additional restrictions

$$c_{12}^2 c_{13}^2 = \frac{2}{3} \tag{8}$$

and

$$s_{12}^2 c_{13}^2 = \frac{1}{3}, \tag{9}$$

where Eqs. (8) and (9) follow from the partial symmetries of the first and second columns, respectively. These predictions arise here from the requirement that G_ν and G_l are embedded in the Discrete Subgroup of SU(3) and need not arise in a more general approach. It is then possible to obtain specific symmetries [35,36] in which the solar angle is a function of a continuous parameter.

Figure 1, shows the correlation plots (thick blue lines) between $\sin^2\theta_{23}$ and δ_{CP} as given by Eqs. (4), (5). Here, the red solid(dashed) contours represent the 3σ allowed region for NH(IH) as obtained from the global-fit data by the Nu-fit Collaboration [63]. Equations (4), (5) give two values of the CP phase (namely, δ_{CP} and $360° - \delta_{CP}$) for each value of θ_{23} except for $\delta_{CP} \equiv 180°$. The width of the blue lines is due to the uncertainty of the angles θ_{12} and θ_{13}, subject to the conditions given in Eqs. (8) and (9), corresponding to Eqs. (4) and (5), respectively. The correlation between $\sin^2\theta_{23}$ and δ_{CP} is opposite in the class of symmetries that give Eq. (4), *vis-à-vis* those that give Eq. (5). The parameters, $\sin^2\theta_{23}$ and δ_{CP}, are correlated between 0°–180° and are

anticorrelated between 180°–360° for Eq. (4). The opposite is true for Eq. (5). We also notice here that Eq. (5) rules out regions around *CP* conserving (i.e., 0°, 180°, 360°) values. Additionally, we observe that, at 3σ, some of the allowed regions of $\sin^2\theta_{23}$ and δ_{CP}, as predicted by the symmetries, are disfavored by the current global-fit data. From the global-fit data, we observe that the region $39° < \delta_{CP} < 125°$ is completely ruled out at 3σ for the NH and the region $\delta_{CP} < 195°$ for the IH. The symmetry predictions can further constrain the values of δ_{CP} presently allowed by the global data.

In the next section, we study how far the allowed areas in the δ_{CP}-$\sin^2\theta_{23}$ plane can be restricted if the simulated experimental data confronts the symmetry predictions.

III. EXPERIMENTAL SPECIFICATIONS

In this paper, we have simulated all of the experiments using the GLoBES package [64,65] along with the required auxiliary files [66,67]. We have considered the experimental setup and the detector performance of DUNE and HK in accordance with Refs. [68] and [69], respectively.

(i) *Deep Underground Neutrino Experiment (DUNE):* The DUNE is a Fermilab based next generation long baseline superbeam experiment. This experiment will utilize the upcoming leading edge facility—the Long Baseline Neutrino Facility (LBNF)—which will provide a high intensity neutrino beam and the infrastructure required for DUNE. In this experiment, the muon-neutrino beam from Fermilab will travel a baseline of 1300 km before it gets detected at the far detector, situated at the Sanford Underground Research Facility (SURF) in Lead, South Dakota. The proposed far detector for DUNE is a liquid argon time-projection chamber (LARTPC) detector with a volume of 40 kT. The beam power will be initially 1.2 MW, and later, it will be increased to 2.3 MW [70]. In our simulation, we consider the neutrino flux [71] corresponding to 1.2 MW beam power, which gives 1×10^{21} protons on target (POT) per year. This corresponds to a proton energy of 120 GeV. We also consider a total run time of $(5\nu + 5\bar{\nu})$ years as proposed by the experiment.

(ii) *Hyper-Kamiokande Experiment:* The Hyper-Kamiokande experiment [69] is a Japanese based long baseline experiment that will use the Japan Proton Accelerator Research Complex (J-PARC) neutrino beam facility. The primary goal of the HK experiment is to determine *CP* violation. However, it is also capable of observing nucleon decay, atmospheric neutrinos, and neutrinos of astronomical origin. Recently, the collaboration has proposed two alternatives for the location of the far detector. The first one is Tokai-to-Hyper-Kamiokande (T2HK), which plans on constructing two water-cherenkov detectors (cylindrical tanks) of fiducial volume 187 kt at 295 km in Kamioka. Alternatively, T2HKK proposes to have one tank of 187 kt at 295 km in Kamioka and the other 187 kt tank at 1100 km in Korea [69]. In our simulations, we have considered the off axis angle (OAA) for this detector in Korea as 1.5°, a proposed run time ratio to be 1:3 in neutrino and antineutrino modes (total run time 10 years), and the proton beam power of 1.3 MW, giving a total of 27×10^{21} protons on target (POT).

IV. PHENOMENOLOGICAL ANALYSIS

In this section, we perform a phenomenological analysis exploring the possibility of probing the correlations C_1 and C_2 at DUNE, T2HK, and T2HKK. This is discussed in terms of correlation plots in the $\sin^2\theta_{23}$-δ_{CP} plane. We also discuss the possibility of distinguishing between the two models at these experiments.

We perform a χ^2 test with χ^2 defined as,

$$\chi^2_{\rm tot} = \min_{\xi,\omega}\{\chi^2_{\rm stat}(\omega,\xi) + \chi^2_{\rm pull}(\xi) + \chi^2_{\rm prior}\}. \quad (10)$$

$\chi^2_{\rm stat}$ is the statistical χ^2, whereas $\chi^2_{\rm pull}$ signifies the systematic uncertainties, which are included using the method of pulls with ξ denoting the pull variable [72–74]. Here, ω represents the oscillation parameters: $\{\sin^2\theta_{23}, \sin^2\theta_{12}, \delta_{CP}, \Delta m^2_{21}, \Delta m^2_{31}\}$. $\chi^2_{\rm prior}$ captures the knowledge of the oscillation parameters from other experiments and is defined as,

$$\chi^2_{\rm prior}(p) = \frac{(p_0 - p)^2}{\sigma_0^2}, \quad (11)$$

p denotes the parameter for which the prior is added, and p_0 and σ_0 correspond to its best fit value and 1σ error, respectively. In our analysis we have considered the effect of the prior on the parameters θ_{13} and θ_{12}. We assume a Poisson distribution to calculate the statistical $\chi^2_{\rm stat}$,

$$\chi^2_{\rm stat} = \sum_i 2\left(N_i^{\rm test} - N_i^{\rm true} - N_i^{\rm true}\log\frac{N_i^{\rm test}}{N_i^{\rm true}}\right). \quad (12)$$

Here, 'i' refers to the number of bins and $N_i^{\rm test}$, $N_i^{\rm true}$ are the total number of events due to test and true sets of oscillation parameters, respectively. $N_i^{\rm test}$ is defined as follows, including the effect of systematics

$$N_i^{\rm (k)test}(\omega,\xi) = \sum_{k=s,b} N_i^{(k)}(\omega)\left[1 + c_i^{(k)\rm norm}\xi^{(k)\rm norm} + c_i^{(k)\rm tilt}\xi^{(k)\rm tilt}\frac{E_i - \bar{E}}{E_{\rm max} - E_{\rm min}}\right], \quad (13)$$

where $k = s(b)$ represent the signal(background) events. $c_i^{\rm norm}(c_i^{\rm tilt})$ corresponds to the change in the number of

events due to the pull variable $\xi^{\rm norm}(\xi^{\rm tilt})$. In the above equation, E_i denotes the mean reconstructed energy of the ith bin with $E_{\rm min}$ and $E_{\rm max}$ representing the maximum and minimum energy in the entire energy range and $\bar{E} = (E_{\rm max} + E_{\rm min})/2$ is the mean energy over this range. The systematic uncertainties (normalization errors) and efficiencies corresponding to signals and backgrounds of DUNE and HK are taken from [41,69]. For DUNE, the signal normalization uncertainties on $\nu_e/\bar{\nu_e}$ and $\nu_\mu/\bar{\nu_\mu}$ are considered to be 2% and 5% respectively. While a range of 5% to 20% background uncertainty along with the correlations among their sources have also been included. On the other hand, for T2HK the signal normalization error on $\nu_e(\bar{\nu_e})$ and $\nu_\mu(\bar{\nu_\mu})$ are considered to be 3.2% (3.9%) and 3.6%(3.6%) respectively. In the case of T2HKK, 3.8% (4.1%) and 3.8% (3.8%) are taken as the signal normalization errors on $\nu_e(\bar{\nu_e})$ and $\nu_\mu(\bar{\nu_\mu})$ respectively. The background normalization uncertainties range from 3.8% to 5%. ${N_i}^{\rm true}$ in Eq. (12) is obtained by adding the simulated signal and background events i.e., ${N_i}^{\rm true} = N_i^s + N_i^b$.

In Table I, we list the values for the neutrino oscillation parameters that we have used in our numerical simulation. These values are consistent with the results obtained from the global fit of world neutrino data [24–26].

A. Testing the $\sin^2\theta_{23}$-δ_{CP} correlation predicted by the symmetries at DUNE, T2HK, and T2HKK

The numerical analysis is performed as follows.

(i) The data corresponding to each experiment is generated by considering the true values of the oscillation parameters given in Table I. Note that the true values of θ_{23} and δ_{CP} are spanned over the range (39–51°) and (0–360°), respectively.

(ii) In the theoretical fit, we calculate the test events by marginalizing over the parameters $\sin^2\theta_{13}$, $|\Delta m^2_{31}|$, $\sin^2\theta_{23}$ and $\sin^2\theta_{12}$ in the test plane using the ranges presented in Table I.

(iii) The test values of δ_{CP} used are as predicted by the symmetries specified in Eq. (4) for C_1 and Eq. (5) in C_2.

TABLE I. Values of oscillation parameters that are considered in this study unless otherwise mentioned. We vary the true values of θ_{23} in the whole allowed range, and marginalization for each $\theta_{23}^{\rm true}$ is done over the full allowed range of θ_{23}. See text for more details.

Osc. param.	True values	Test values
$\sin^2\theta_{13}$	0.0219	0.0197–0.0244
$\sin^2\theta_{12}$	0.306	0.272–0.346
θ_{23}	39°–51°	39°–51°
$\Delta m^2_{21}(\mathrm{eV}^2)$	7.50×10^{-5}	Fixed
$\Delta m^2_{31}(\mathrm{eV}^2)$	2.50×10^{-3}	$(2.35\text{–}2.65)\times10^{-3}$
δ_{CP}	(0–360)°	Symmetry predictions

(iv) In addition we impose the conditions given in Eq. (8) for the symmetry relation C_1 and Eq. (9) for symmetry relation C_2 in the test. Note that given the current range of $\sin^2\theta_{13}$ these relations restrict the value of $\sin^2\theta_{12}$ to $0.316 < \sin^2\theta_{12} < 0.319$ for C_1 and $\sin^2\theta_{12}$ to $0.34 < \sin^2\theta_{12} < 0.342$ for C_2. These values of $\sin^2\theta_{12}$ are within the current 3σ allowed range. Note that these ranges exclude the current best-fit value of $\sin^2\theta_{12}$. Precise measurement of θ_{12}, for instance, in the reactor neutrino experiment JUNO [75], can provide a stringent test of these scenarios.

(v) We have not added any prior in this analysis. We have checked that the prior on θ_{13} does not play any role when the constraints represented by Eqs. (8) and (9) are applied. In addition, since the best-fit θ_{12} is excluded already by the constraints, the imposition of θ_{12} prior will disfavor the scenarios.

(vi) We minimize the χ^2 and plot the regions in the $\sin^2\theta_{23}(\mathrm{true})$-$\delta_{CP}(\mathrm{true})$ plane for which $\chi^2 \leq \chi^2_{\rm min} + \Delta\chi^2$ where $\Delta\chi^2$ values used correspond to 1σ, 2σ, and 3σ.

The resultant plots are shown in Fig. 2 for true hierarchy as NH and Fig. 3 for true hierarchy as IH. We assume the hierarchy to be known, and we do not marginalize over hierarchy.[3] The blue, gray, and yellow bands in Figs. 2 and 3 represent 1σ, 2σ, 3σ regions in the $\sin^2\theta_{23}$-δ_{CP} plane, respectively. The red contours show the 3σ allowed area obtained by the Nu-fit Collaboration [26,63]. These plots show the extent to which these three experiments can test the correlations between the two yet undetermined variables $\sin^2\theta_{23}$ and δ_{CP} in conjunction with the symmetry predictions. The red contours show the 3σ allowed area obtained by the Nu-fit Collaboration [26,63]. The topmost panel corresponds to DUNE 40 kT detector whereas the middle and the lowest panels correspond to T2HK and T2HKK experiments, respectively. The left plots in all the rows are for testing C_1 whereas the right plots are for testing C_2.

The figures show that, because of the correlations predicted by symmetries, certain combinations of the true θ_{23} and δ_{CP} values get excluded by DUNE, T2HK and T2HKK. Owing to their high sensitivity to determine CP violation, T2HK and T2HKK constrain the range of δ_{CP} better than that of DUNE. This can be seen from the figures (see Figs. 2,3) which show that, as we go from top to bottom the contours gets thinner with respect to δ_{CP}. For instance, for the C_1 correlation, the CP conserving values 0° and 360° get excluded at 3σ for both of the octants by all three experiments, as can be seen from the plots in the left panels. However, for the C_2, these values are allowed at 3σ

[3]We verified that there is less of an effect of marginalizing over the hierarchy. Hence, to save the computation time, we have presented the plots by assuming that the hierarchy is known.

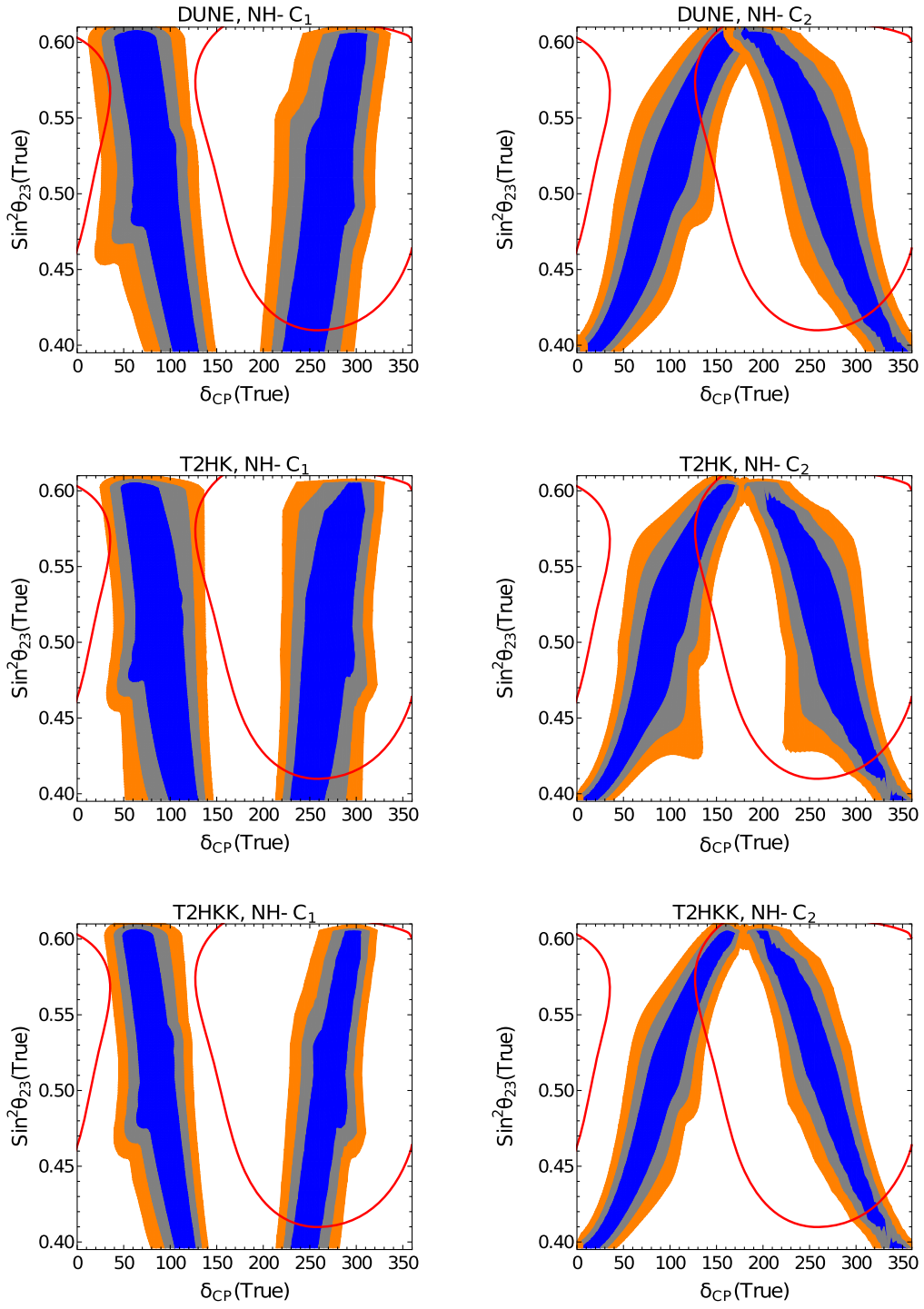

FIG. 2. Contour plots in the true: $\sin^2\theta_{23}$(true)-δ_{CP}(true) plane for DUNE, T2HK, and T2HKK. The left(right) panel represents the prediction from the symmetry relation $C_1(C_2)$ which corresponds to the Eq. (4) [Eq. (5)]. The hierarchy is fixed as NH. The red contour in each panel represents the 3σ allowed area from the global analysis of neutrino oscillation data as obtained by the Nu-fit Collaboration [26,63] for the normal hierarchy. The blue, gray, and yellow shaded contours correspond to 1σ, 2σ, and 3σ respectively.

for all three experiments. Whereas, $\delta_{CP} = 0°$ and $360°$ are excluded by DUNE and HK experiments at 1σ and 2σ, respectively. Again, one can see from the right panels that for C_2, $\delta_{CP} = 180°$ is allowed for $\sin^2\theta_{23} > 0.55$ (i.e., higher octant) by DUNE but barely gets excluded at 2σ by the T2HK and T2HKK experiments. The correlations predicted by the symmetry considerations being independent of hierarchy, the allowed regions are not very different for NH and IH, but the region of parameter space allowed by the current data for IH is more constrained and the

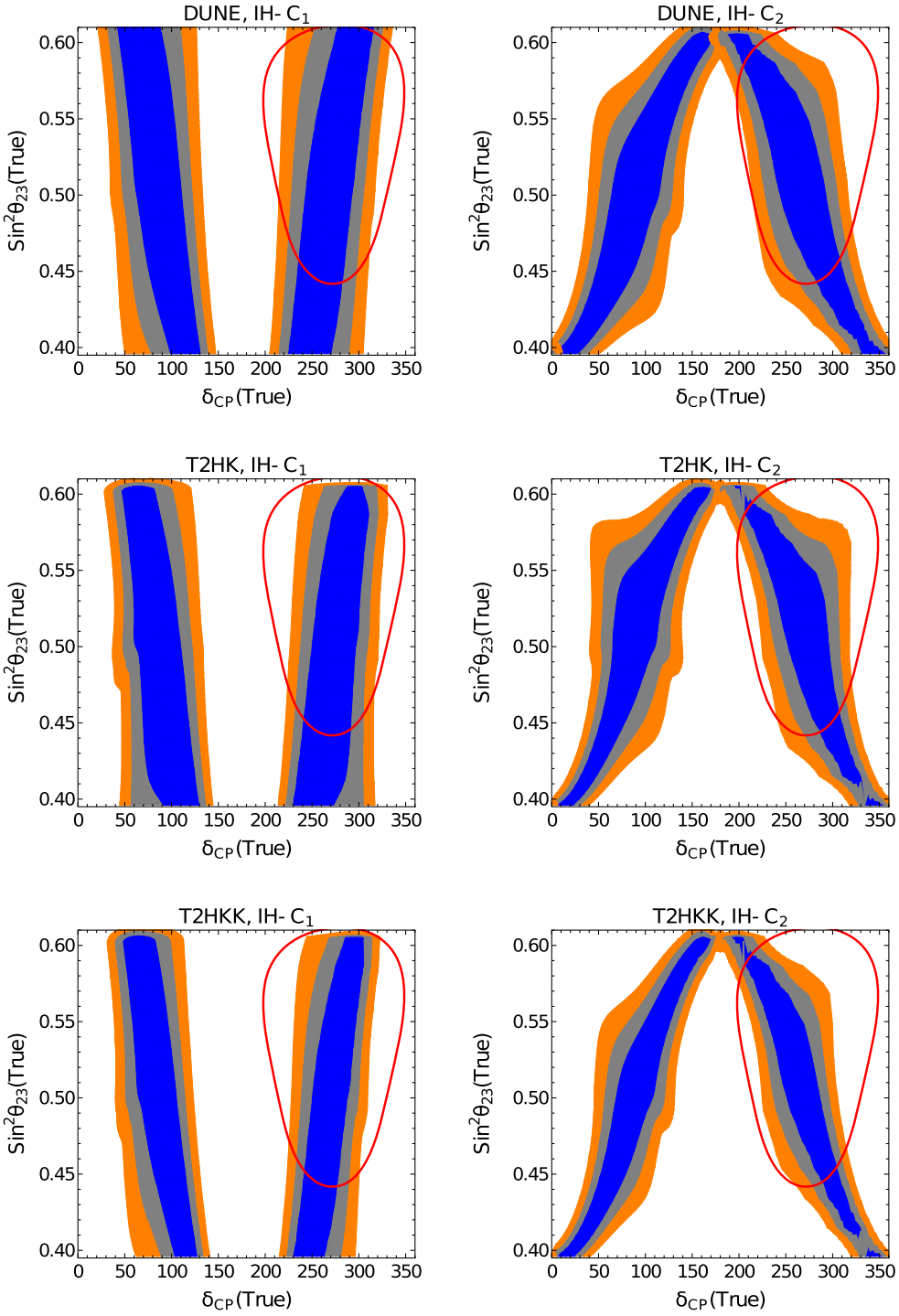

FIG. 3. Same as Fig. 2 but for inverted hierarchy.

symmetry predictions restrict it further, as can be seen from Fig. 3. Some of the parameter space allowed by the current data can also be disfavored by incorporating the correlations due to symmetry relations.

In Sec. II, it was discussed that the additional restrictions, Eqs. (8) and (9), are obtained when the partial μ-τ symmetry is derived in the specific approach discussed. However, possibilities exist where partial μ-τ symmetry can be generated without the additional restrictions. In this context, we analyzed the changes in the allowed areas when the additional restrictions are not imposed. This is done only for DUNE, which captures the essential trend of the impact of not imposing the extra constraints. This is shown in Fig. 4. We have studied this for the representative case of the symmetry relation C_2. The procedure for generating the plots is the same as outlined earlier, except with the

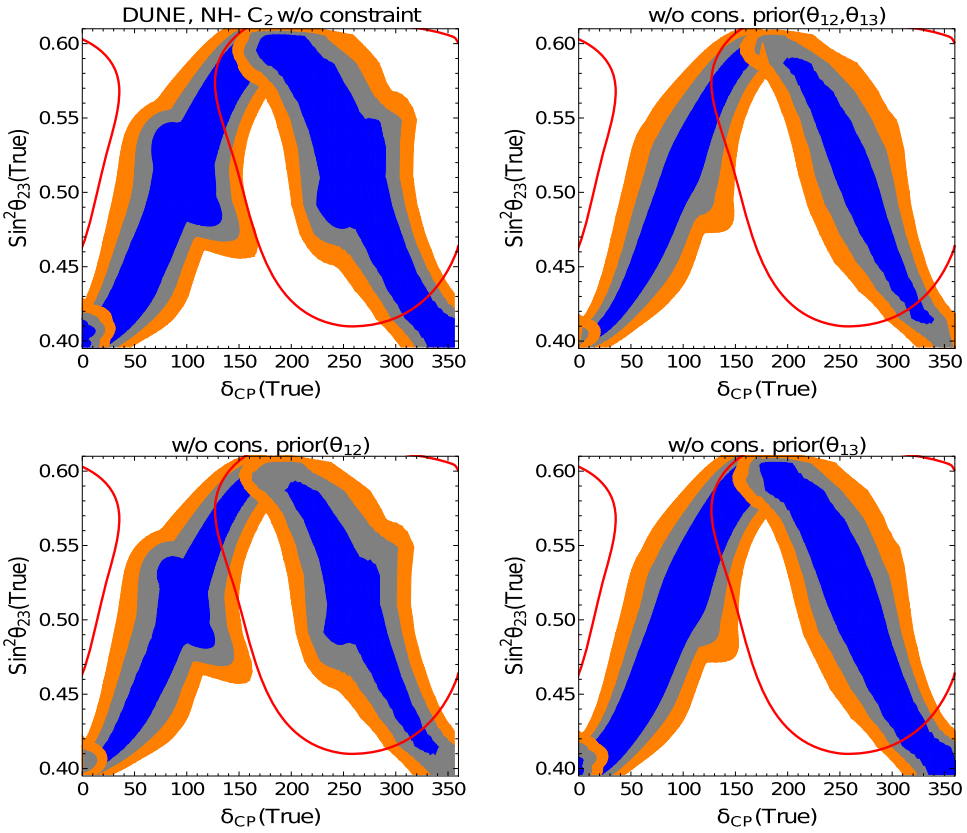

FIG. 4. Contour plots in the true: $\sin^2\theta_{23}$(true)-δ_{CP}(true) plane for DUNE, assuming the symmetry relation C_2 in the test. The additional constraints, Eq. (9), have not been applied in generating this plot. The first panel represents the plot without including any prior. The second panel in the first row shows the effect of the prior on θ_{12} and θ_{13}. The first plot in the second row shows the effect of the inclusion of the θ_{12} prior, whereas the second plant shows the effect of the inclusion of the θ_{13} prior. The hierarchy is fixed as NH. The red contour in each panel represents the 3σ allowed area of the Nu-fit Collaboration.

inclusion of the priors. While the earlier plots were generated without any prior, for these cases, we have studied the following scenarios:

(1) No prior on θ_{13} and θ_{12}.
(2) Prior on θ_{13} and θ_{12}.
(3) Prior on θ_{12} and no prior θ_{13}.
(4) Prior on θ_{13} and no prior θ_{12}.

The first plot of top row is without any prior on the parameters θ_{12} and θ_{13} and no additional constraints imposed. We find that the allowed area increases in size as compared to the cases where the extra constraints embodied in Eqs. (8) and (9) are not imposed. The second

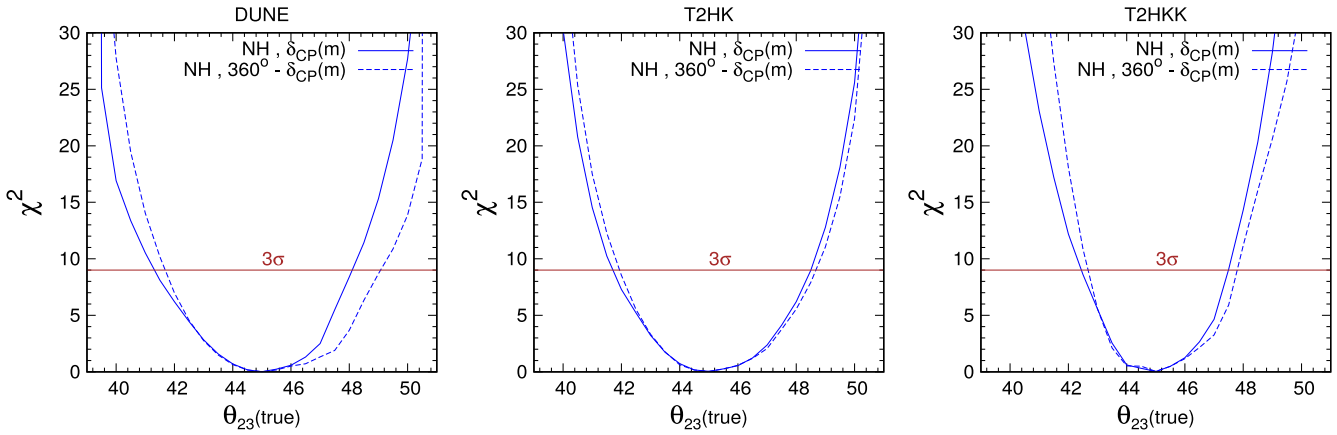

FIG. 5. The sensitivity of DUNE, T2HK, and T2HKK experiments to differentiate between C_1 and C_2 correlations for known normal hierarchy.

TABLE II. The limits of θ_{23} in degrees below and above which the correlations C_1 and C_2 can be differentiated at 3σ C.L. for two different ranges of δ_{CP}.

Range of δ_{CP}	DUNE		T2HK		T2HKK	
$0° \le \delta_{CP} \le 180°$	$\theta_{23} \le 41.5°$	$\theta_{23} \ge 48°$	$\theta_{23} \le 41.8°$	$\theta_{23} \ge 48.5°$	$\theta_{23} \le 42.6°$	$\theta_{23} \ge 47.5°$
$180° \le \delta_{CP} \le 360°$	$\theta_{23} \le 41.8°$	$\theta_{23} \ge 49°$	$\theta_{23} \le 42°$	$\theta_{23} \ge 48.7°$	$\theta_{23} \le 42.8°$	$\theta_{23} \ge 47.7°$

plot of top row is without imposing these additional restrictions, but including the prior on θ_{12} and θ_{13}. In this case, the allowed regions are more restricted and certain combinations of θ_{23} and δ_{CP} get disfavored. We proceed further to show the impact of the prior considering a single mixing angle at a time in the second row. In the first plot of the bottom row, we show the effect of including the prior on θ_{12} but no prior on θ_{13}. In this case, the shape of the allowed regions are same but they reduce in size. The effect of certain combination of θ_{23} and δ_{CP} values getting disfavored are seen more at the 1σ level. Similarly, the second plot of the bottom row shows the effect of the θ_{13} prior. In this case also, the allowed regions reduce in size as compared to the case where no priors are included (first panel of top row).

B. Differentiating between the C_1 and C_2 symmetries

In this subsection, we explore the possibility of differentiation between the symmetries C_1 and C_2. This is presented in Fig. 5, where we plot $\Delta\chi^2$ vs true θ_{23}. To find $\chi^2_{\rm stat}$ [as defined in Eq. (12)], true events are calculated by varying the true values of θ_{23} in the range (39°–51°). For each true θ_{23}, true values of $\sin^2\theta_{13}$ and $\sin^2\theta_{12}$ are allowed to vary in their 3σ range such that the condition as given in Eq. (8) is satisfied. Using these true values of the angles the true δ_{CP} values are calculated using the correlation C_1. This leads to two sets of true events corresponding to δ_{CP} and $(360° - \delta_{CP})$, respectively. The remaining oscillation parameters are kept fixed at their best-fit values as shown in Table I. In the theoretical fit, to calculate test events, we marginalize over $\sin^2\theta_{13}$, $|\Delta m^2_{31}|$, $\sin^2\theta_{23}$ in the range given in Table I, and test δ_{CP} values are calculated using the C_2. In addition, we impose the condition as given in Eq. (9), connecting test $\sin^2\theta_{23}$ and $\sin^2\theta_{13}$ and compute the χ^2. For each choice of true $\sin^2\theta_{23}$, the χ^2 is marginalized over the true $\sin^2\theta_{13}$ and $\sin^2\theta_{12}$, and the minimum χ^2 for each true $\sin^2\theta_{23}$ is taken as the value of χ^2. This process is done for both δ_{CP} and $360°$–δ_{CP} separately. We have performed the analysis considering the true hierarchy as NH. We have checked that if we assume the IH as the true hierarchy, we obtain similar results. The three panels from left to right represent DUNE, T2HK, and T2HKK, respectively. The solid blue curves in the plots are for the predicted range $\delta_{CP} \in (0° < \delta_{CP} < 180°)$, and the dashed blue curves in the plots are for complementary range $360°$–$\delta_{CP} \in (180° < \delta_{CP} < 360°)$ as predicted by the correlations. The brown solid line shows the 3σ C.L. We observe from the figure that at the maximal θ_{23}, both of the correlations are indistinguishable by all the three experiments as is expected from Eqs. (4), (5).

The capability of the experiments to differentiate between the two correlations increases as we move away from the maximal value. The range of θ_{23}, for which the three experiments can differentiate between the correlations at 3σ, is given in Table II. The lower limits signify the values of θ_{23} below which the correlations can be differentiated at 3σ, and the upper limits are for the values above which the same can be achieved.

V. CONCLUSION

We study here partial μ-τ reflection symmetry of the leptonic mixing matrix, U, which can arise from discrete flavor symmetry. Specific assumptions which lead to this symmetry were reviewed here. This symmetry implies $|U_{\mu i}| = |U_{\tau i}| (i = 1, 2, 3)$ for a single column of the leptonic mixing matrix U. If this is true for the third column of U, then it leads to maximal value of the atmospheric mixing angle and CP phase δ_{CP}. However, if this is true for the first or the second column, then one obtains definite correlations among θ_{23} and δ_{CP}. We call these scenarios C_1 (equality for the first column) and C_2 (equality of the second column). We find that almost all the discrete subgroups of SU(3), except a few exceptional cases having three dimensional irreducible representations, display the form of partial μ-τ symmetry. We study the correlations among θ_{23} and δ_{CP} in the two scenarios. Each scenario gives two values of δ_{CP} for a given θ_{23}—one belonging to $0° < \delta_{CP} < 180°$ and the other belonging to $180° < \delta_{CP} < 360°$. The models also give specific correlations between θ_{23} and δ_{CP} and these are opposite for C_1 and C_2. We study how the allowed areas in the $\sin^2\theta_{23}$-δ_{CP} plane obtained by the global analysis of neutrino oscillation data from the Nu-Fit Collaboration compare with the predictions from the symmetries.

We also expound the testability of these symmetries considering next generation accelerator based experiments, DUNE and Hyper-Kamiokande. This is illustrated in terms of plots in the $\sin^2\theta_{23}$(true)-δ_{CP}(true) plane obtained by fitting the simulated experimental data with the symmetry predictions for δ_{CP}. The values of θ_{23} are found to be more constrained for the CP conserving values namely $\delta_{CP} = 0°$, 180°, 360°. For the C_2 correlation, the θ_{23} is found to be in the higher octant for $\delta_{CP} = 180°$ and in the lower octant for $\delta_{CP} = 0°$ and 360°. For the correlation C_1, values of δ_{CP}

around all the three CP conserving values $\delta_{CP} = 0°$, 180°, and 360° are seen to be disfavored. Finally, we illustrate the capability of DUNE and Hyper-Kamiokande to distinguish between the predictions of the two correlations. We observe that both the experiments can better differentiate between these two as one moves away from the maximal θ_{23} value.

In conclusion, the future experiments provide testing grounds for various symmetry relations, specially those connecting θ_{23} and δ_{CP}.

ACKNOWLEDGMENTS

The research work of A. S. J. was supported by BRNS (Department of Atomic Energy) and by Department of Science and Technology, Government of India through the Raja Ramanna fellowship and the J. C. Bose Grant, respectively. N. N. gratefully acknowledges the support in part by the National Natural Science Foundation of China under Grant No. 11775231 for the research work.

[1] G. Altarelli and F. Feruglio, Rev. Mod. Phys. **82**, 2701 (2010).
[2] G. Altarelli, F. Feruglio, and L. Merlo, Fortschr. Phys. **61**, 507 (2013).
[3] A. Yu. Smirnov, J. Phys. Conf. Ser. **335**, 012006 (2011).
[4] H. Ishimori, T. Kobayashi, H. Ohki, Y. Shimizu, H. Okada, and M. Tanimoto, Prog. Theor. Phys. Suppl. **183**, 1 (2010).
[5] S. F. King and C. Luhn, Rep. Prog. Phys. **76**, 056201 (2013).
[6] P. F. Harrison and W. G. Scott, Phys. Lett. B **547**, 219 (2002).
[7] W. Grimus and L. Lavoura, Phys. Lett. B **579**, 113 (2004).
[8] P. M. Ferreira, W. Grimus, L. Lavoura, and P. O. Ludl, J. High Energy Phys. 09 (2012) 128.
[9] W. Grimus and L. Lavoura, Fortschr. Phys. **61**, 535 (2013).
[10] R. N. Mohapatra and C. C. Nishi, Phys. Rev. D **86**, 073007 (2012).
[11] E. Ma, A. Natale, and O. Popov, Phys. Lett. B **746**, 114 (2015).
[12] A. S. Joshipura and K. M. Patel, Phys. Lett. B **749**, 159 (2015).
[13] A. S. Joshipura, J. High Energy Phys. 11 (2015) 186.
[14] A. S. Joshipura and N. Nath, Phys. Rev. D **94**, 036008 (2016).
[15] C. C. Nishi and B. L. Snchez-Vega, J. High Energy Phys. 01 (2017) 068.
[16] Z.-h. Zhao, J. High Energy Phys. 09 (2017) 023.
[17] Z.-C. Liu, C.-X. Yue, and Z.-h. Zhao, J. High Energy Phys. 10 (2017) 102.
[18] Z.-z. Xing, D. Zhang, and J.-y. Zhu, J. High Energy Phys. 11 (2017) 135.
[19] Z.-z. Xing and J.-y. Zhu, Chin. Phys. C **41**, 123103 (2017).
[20] A. S. Joshipura, arXiv:1801.02843.
[21] N. Nath, Z.-z. Xing, and J. Zhang, Eur. Phys. J. C **78**, 289 (2018).
[22] Z.-h. Zhao, Nucl. Phys. **B935**, 129 (2018).
[23] C. Patrignani *et al.* (Particle Data Group), Chin. Phys. C **40**, 100001 (2016).
[24] P. F. de Salas, D. V. Forero, C. A. Ternes, M. Tortola, and J. W. F. Valle, Phys. Lett. B **782**, 633 (2018).
[25] F. Capozzi, E. Lisi, A. Marrone, D. Montanino, and A. Palazzo, Nucl. Phys. **B908**, 218 (2016).
[26] I. Esteban, M. C. Gonzalez-Garcia, M. Maltoni, I. Martinez-Soler, and T. Schwetz, J. High Energy Phys. 01 (2017) 087.
[27] T. Fukuyama and H. Nishiura, arXiv:hep-ph/9702253.
[28] E. Ma and M. Raidal, Phys. Rev. Lett. **87**, 011802 (2001); **87**, 159901(E) (2001).
[29] C. S. Lam, Phys. Lett. B **507**, 214 (2001).
[30] K. R. S. Balaji, W. Grimus, and T. Schwetz, Phys. Lett. B **508**, 301 (2001).
[31] W. Grimus, A. S. Joshipura, S. Kaneko, L. Lavoura, H. Sawanaka, and M. Tanimoto, Nucl. Phys. **B713**, 151 (2005).
[32] A. S. Joshipura, Eur. Phys. J. C **53**, 77 (2008).
[33] Z.-z. Xing and Z.-h. Zhao, Rep. Prog. Phys. **79**, 076201 (2016).
[34] Z.-z. Xing and S. Zhou, Phys. Lett. B **737**, 196 (2014).
[35] S.-F. Ge, D. A. Dicus, and W. W. Repko, Phys. Lett. B **702**, 220 (2011).
[36] S.-F. Ge, D. A. Dicus, and W. W. Repko, Phys. Rev. Lett. **108**, 041801 (2012).
[37] S. T. Petcov, Eur. Phys. J. C **78**, 709 (2018).
[38] R. de Adelhart Toorop, F. Feruglio, and C. Hagedorn, Phys. Lett. B **703**, 447 (2011).
[39] A. D. Hanlon, S.-F. Ge, and W. W. Repko, Phys. Lett. B **729**, 185 (2014).
[40] A. D. Hanlon, W. W. Repko, and D. A. Dicus, Adv. High Energy Phys. **2014**, 469572 (2014).
[41] R. Acciarri *et al.* (DUNE Collaboration), arXiv:1512.06148.
[42] V. Barger, A. Bhattacharya, A. Chatterjee, R. Gandhi, D. Marfatia, and M. Masud, Phys. Rev. D **89**, 011302 (2014).
[43] S. K. Agarwalla, S. Prakash, and S. Uma Sankar, J. High Energy Phys. 03 (2014) 087.
[44] V. Barger, A. Bhattacharya, A. Chatterjee, R. Gandhi, D. Marfatia, and M. Masud, Int. J. Mod. Phys. A **31**, 1650020 (2016).
[45] K. Bora, D. Dutta, and P. Ghoshal, Mod. Phys. Lett. A **30**, 1550066 (2015).
[46] M. Ghosh, S. Goswami, and S. K. Raut, Eur. Phys. J. C **76**, 114 (2016).
[47] D. Dutta and k. Bora, Mod. Phys. Lett. A **30**, 1550017 (2015).
[48] K. N. Deepthi, C. Soumya, and R. Mohanta, New J. Phys. **17**, 023035 (2015).
[49] N. Nath, M. Ghosh, and S. Goswami, Nucl. Phys. **B913**, 381 (2016).
[50] R. Srivastava, C. A. Ternes, M. Trtola, and J. W. F. Valle, Phys. Rev. D **97**, 095025 (2018).
[51] P. Pasquini, Adv. High Energy Phys. **2018**, 1825874 (2018).

[52] R. Srivastava, C. A. Ternes, M. Trtola, and J. W. F. Valle, Phys. Lett. B **778**, 459 (2018).
[53] S. K. Agarwalla, S. S. Chatterjee, S. T. Petcov, and A. V. Titov, Eur. Phys. J. C **78**, 286 (2018).
[54] S. S. Chatterjee, M. Masud, P. Pasquini, and J. W. F. Valle, Phys. Lett. B **774**, 179 (2017).
[55] S. T. Petcov and A. V. Titov, Phys. Rev. D **97**, 115045 (2018).
[56] P. Ballett, S. F. King, S. Pascoli, N. W. Prouse, and T. Wang, J. High Energy Phys. 03 (2017) 110.
[57] P. Ballett, S. Pascoli, and J. Turner, Phys. Rev. D **92**, 093008 (2015).
[58] P. Ballett, S. F. King, C. Luhn, S. Pascoli, and M. A. Schmidt, J. High Energy Phys. 12 (2014) 122.
[59] J. T. Penedo, S. T. Petcov, and T. Yanagida, Nucl. Phys. **B929**, 377 (2018).
[60] S. F. King and T. Neder, Phys. Lett. B **736**, 308 (2014).
[61] A. S. Joshipura and K. M. Patel, J. High Energy Phys. 01 (2017) 134.
[62] W. Grimus and P. O. Ludl, J. Phys. A **47**, 075202 (2014).
[63] NuFIT, NuFIT 3.2, http://www.nu-fit.org/.
[64] P. Huber, M. Lindner, and W. Winter, Comput. Phys. Commun. **167**, 195 (2005).
[65] P. Huber, J. Kopp, M. Lindner, M. Rolinec, and W. Winter, Comput. Phys. Commun. **177**, 432 (2007).
[66] M. D. Messier, Ph.D. thesis, Boston University, 1999.
[67] E. Paschos and J. Yu, Phys. Rev. D **65**, 033002 (2002).
[68] T. Alion *et al.* (DUNE Collaboration), arXiv:1606.09550.
[69] K. Abe *et al.* (hyper-Kamiokande Proto-Collaboration), Prog. Theor. Exp. Phys. **2018**, 063C01 (2018).
[70] C. Adams *et al.* (LBNE Collaboration), arXiv:1307.7335.
[71] D. Cherdack, Private communication (2014).
[72] M. C. Gonzalez-Garcia and M. Maltoni, Phys. Rev. D **70**, 033010 (2004).
[73] G. Fogli, E. Lisi, A. Marrone, D. Montanino, and A. Palazzo, Phys. Rev. D **66**, 053010 (2002).
[74] R. Gandhi, P. Ghoshal, S. Goswami, P. Mehta, S. Uma Sankar, and S. Shalgar, Phys. Rev. D **76**, 073012 (2007).
[75] Y.-F. Li (JUNO Collaboration), in *Proceedings, 17th Lomonosov Conference on Elementary Particle Physics: Moscow, Russia, 2015* (2017), pp. 27–33 [arXiv:1606.04743], https://inspirehep.net/record/1469449/files/arXiv:1606.04743.pdf.